Identification and characterisation of performance limiting defects and cell mismatch in photovoltaic modules

Jacqui L Crozier

Ernest E van Dyk

Frederick J Vorster

Department of Physics, Nelson Mandela Metropolitan University, Port Elizabeth, South Africa

Abstract

The performance and longevity of photovoltaic (PV) modules can be severely limited by cell mismatch occurring when a solar cell in a series-connected string produces a lower current than the other cells in that string. The current output of the entire string is limited by the weakest cell in the string so shading or damage to a single cell in a module can affect the entire module's current output. Electroluminescence (EL) occurs when a positive current and voltage are applied to a solar cell and is used to identify damage and defects in the cell. In this study, the cell mismatch in three single crystalline silicon modules was investigated using EL and current-voltage (I-V) characterisation techniques. Two modules have a white discolouration that affects the majority of the cells in the module and also have signs of mechanical damage, while the third module acts as a reference as it has no discolouration and appears undamaged. The EL signal intensity is related to cell performance and identifies material defects, bad contacts and broken cells. Cell mismatch in a module results in a decrease in the performance parameters obtained from the I-V characteristic curve of the module. The I-V curves indicate the presence of current mismatch in the degraded modules, which is supported by the EL images of these modules. The use of EL images, in conjunction with the I-V curves, allows the degradation in the modules to be characterised.

Keywords: photovoltaics, cell mismatch, current-voltage characterisation, electroluminescence, degradation

1. Introduction

The reliability and longevity of photovoltaic (PV) modules is a key factor in the success of solar energy as an alternative energy source. Cell mismatch arises from unbalanced current production of some cells in a series-connected string. This mismatch results from degradation in the cell due to mechanically damaged cells or shading due to shadows or the accumulation of dirt (Meyer and van Dyk, 2004). Cell mismatch affects the current production of the cell and, hence, the string.

The objectives of this investigation are to identify and characterise cell mismatch in PV modules by comparing the results of the current-voltage (I-V) characteristics with electroluminescence (EL) images. EL is a useful solar cell characterisation technique as it is fast, non-destructive and sensitive to the effects of shunt and series resistances and recombination parameters. This luminescence is dependent on the optical, electrical and resistive properties of the solar cell.

EL imaging is very effective in detecting defects in modules such as cracks, broken fingers and broken cells (Mansouri *et al.*, 2012). For this reason, it is extensively integrated into module production lines and module testing systems and highlights features that are missed during visual inspection (Camino-Villacorta *et al.*, 2012). The EL images allow defective cells in a module to be identified and these defects can be related to reduced output power.

1.1. Current-voltage (I-V) characteristics and cell mismatch

Cell mismatch has a substantial effect on the current-voltage (I-V) curve of the whole module. A cell with a current output lower than the rest of the cells in the string of series-connected cells is referred to

as a 'weak cell'. When cells are connected in series, the voltages of the individual cells add and the total current is limited by the weakest cell.

Figure 1(a) shows a representation of two cells connected in series and the cells are current matched, so the total current flowing through the circuit is equal to the current generated by each cell. At short-circuit the voltage of each cell is zero. Figure 1(b) illustrates the I-V curves of the two cells and how they are combined, with the voltages of each cell adding and the short-circuit current (Isc) is equal to the Isc of each cell. The curves were plotted using a modelling programme called PVSim (King *et al.,* 1996) which includes a statistical variation of parameters of the cells resulting in the I-V curves of cell 1 and cell 2 being slightly different.

If a cell is shaded by leaves or dirt it generates less current than the other cells in the series-connected string, as illustrated in Figure 2(a). Under short-circuit conditions cells 2 and 3 generate current, I, however the current that can flow through the circuit is limited by cell 1, which is only generating half as much current, ½I, thus the excess current flows through the diodes in cells 2 and 3, forward biasing them. At short-circuit the voltages of all the cells must add up to zero and since cells 2 and 3 are forward biased, cell 1 is reverse biased by an equivalent voltage. Cell 1 thus changes from a power generator to a power dissipater (Vorster and van Dyk, 2005). The cell generates heat that may damage the cell by creating a hot-spot which can cause the cell to crack or delaminate from the encapsulation material. The combined output of the series connected cells is dependent on the reverse voltage behaviour of the weak cell (Alonso-García and Ruíz, 2006). Figure 2(b) illustrates the effect on the I-V curve of the weak cell, the Isc of the series connected string is limited by the weak cell.

The effects of cell mismatch can be mitigated by using bypass diodes connected in parallel over a series connected cell or string of cells, illustrated in Figure 3(a). The bypass diode is activated when the weak cell is reverse biased by a voltage equal to the transmission voltage of the diode (Vorster and van Dyk, 2005). Cells 2 and 3 are only slightly forward biased and the current of the series-connected

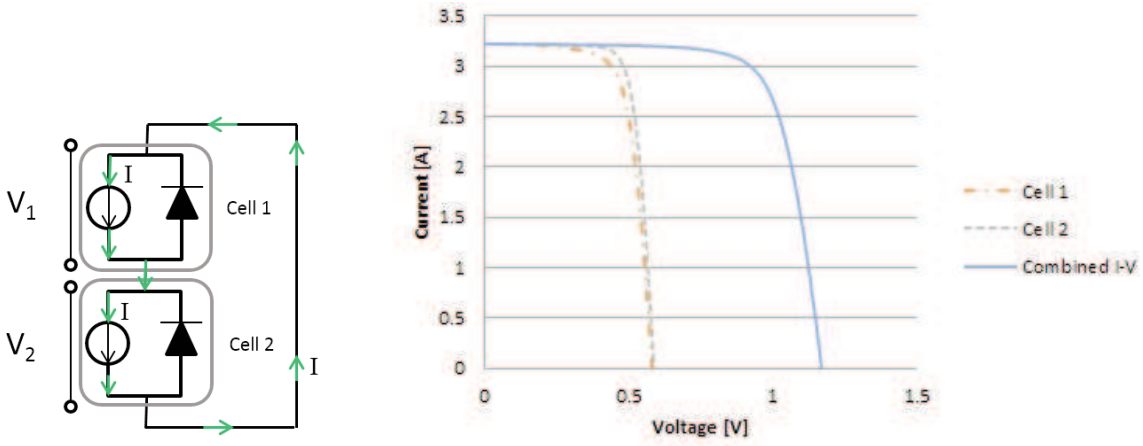

Figure 1: a) The equivalent circuit of two matched solar cells in short-circuit. b) Simulation of the I-V curves of two matched cells and their combined I-V curve. The curves were plotted using a modelling programme called PVSim[2], which includes a statistical variation of parameters of the cells resulting in the I-V curves of cell 1 and cell 2 being slightly different

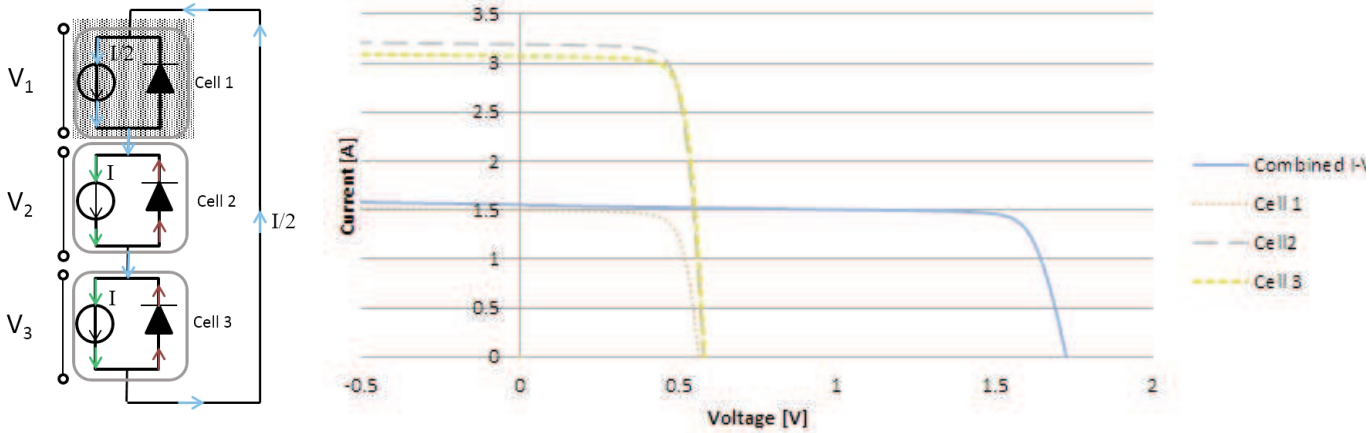

Figure 2: a) The equivalent circuit of three cells in series with one shaded cell. b) The simulated I-V curves of the three cells and the combined I-V curve of all the cells in series

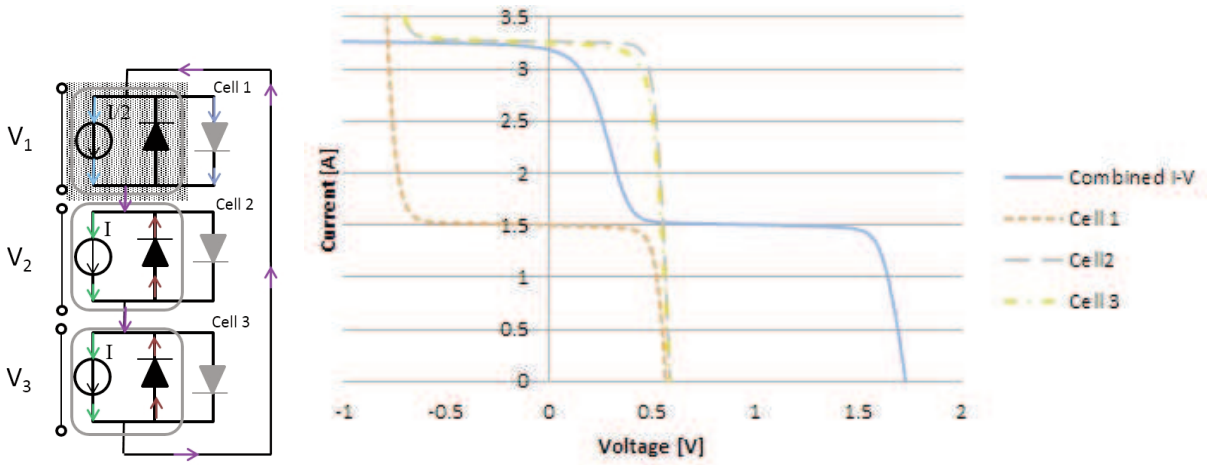

Figure 3: a) The equivalent circuit of three cells in series with one shaded cell with bypass diodes connected in parallel across each cell. b) The simulated I-V curves of the three cells and the combined I-V curve of all the cells in series

string is not limited by cell 1. The activation of the bypass diode results in a step in the I-V curve visible in Figure 3(b). The relative position of the step in the I-V curve is related to the behaviour of the weak cell in reverse bias (Alonso-García and Ruíz, 2006). When cells are connected together in modules, it is impractical to have bypass diodes over each cell so they are connected over strings of series-connected cells.

1.2. Electroluminescence

A solar cell or a LED can be represented as a device with electrical or optical terminals, (Kirchartz *et al.*, 2009). A solar cell receives an optical input in the form of the incoming light and outputs an electrical current. Conversely, a LED receives an electrical input resulting in an optical output. EL occurs in a solar cell when it is forward biased, receiving an electrical input and outputs an electromagnetic emission spectrum. The emission spectrum from silicon is in the infrared region of the electromagnetic spectrum. Luminescence is defined as the emission of light not due to heating so electroluminescence is the emission of light due to an applied bias.

When a silicon solar cell is forward biased, the applied potential difference injects additional carriers into the junction. When some of the carriers recombine radiatively, energy is emitted in the form of electromagnetic radiation, EL, in a range of 1000 to 1200 nm. The intensity of the EL signal is related to the material properties such as the surface recombination velocity, minority carrier lifetime and diffusion length (Fuyuki *et al.*, 2005; Fuyuki *et al.*, 2007; W□rfel *et al.*, 2007; Fuyuki and Kitiyanan, 2008). Extrinsic defects that have occurred in the cell or module during the manufacturing process can also be detected as they result in areas of low or absent EL signal. The EL signal is detected using a cooled silicon charge-coupled device (CCD) camera which provides a grey scale spatial representation of defects in the cell. EL imaging is a very fast, efficient and non-destructive technique for identifying the causes of cell mismatch in PV modules.

Since the initial research of EL of silicon solar cells was completed by Fuyaki *et. al.* (2005), EL has developed into a very successful defect identification and module characterising technique (Mansouri *et al.*, 2012; IEAPVPS, 2014). EL can effectively identify the micro-cracks that are not detected during visual inspection. Micro-cracks can occur during the soldering process (Gabor *et al.*, 2006), during the handling and installation of the modules (Sander *et al.*, 2013; Köntges *et al.*, 2014). The occurrence and distribution of icro-cracks has also been studied in detail (Köntges *et al.*, 2011; Paggi and Sapora, 2013; Kajari-Schröder *et al.*, 2011). Similarly breaks in contact finger, which run perpendicular to the busbars across the cell, are visible in EL. A break across the finger results in that area of the cell having decreased electrical contact. These defects are visible in the EL image as the area around the broken finger appears darker in the image (Chaturvedi *et al.*, 2013; Mansouri *et al.*, 2012). The busbars and solder strapping in a cell provides electrical contact to the cells.

2. Experimental procedure

I-V curves were measured using a calibrated outdoor I-V tracer, which consists of a programmable power supply and an electronic load that allows the output current to be measured through a range of voltages. The current produced by the module is measured at each applied voltage and these data points are plotted as the characteristic I-V curve of the module. The irradiance and the back-of-module temperature were measured during the I-V curve measurements and the results were corrected to standard operating conditions of 25°C and 1000 W/m^2. I-V curves of the modules were measured with and without bypass diodes and the I-V curves

of the individual strings were measured, allowing the current mismatch in the module to be fully identified and characterised.

The EL images were measured by applying a forward bias of 30 V such that a current greater than Isc passes through the module, in this case approximately 4 A. The wavelength of the emitted luminescence of a silicon sample has a peak at about 1150 nm and a portion of this peak can be detected by a silicon CCD camera which has a detection range of 300-1000 nm. The camera's CCD chip is cooled to -50 °C to improve the signal-to-noise ratio. In order for the electroluminescence signal to be detected, the setup must be placed in a dark room to prevent ambient light from being detected. The CCD camera is fitted with an infrared filter and an objective lens for focusing. The module is forward biased using a DC power supply and the CCD camera is connected to a computer with camera control software. The exposure time for each image is about 2.5 seconds. ImageJ (NIH, 2004), image processing software was used to analyse the EL images.

Three single crystalline silicon modules were used in this investigation, all with the same cell material and configuration. Photographs of the three modules are shown in Figure 4. The modules are labelled 1, 2 and 3 with module 1 serving as a reference. The modules have 44 cells connected in two strings of 22 series-connected cells with bypass diodes connected in parallel across the strings. Two of the modules have a visible grey-white discolouration affecting the majority of the cells in the module. This is thought to be due to degradation in the anti-reflective coating on the cell surfaces. The effects of this degradation can be determined by comparing these modules with a third reference module that has no visible degradation. The modules have a specified maximum power (P_{max}) of 65 W, open circuit voltage (V_{oc}) of 25 V and short-circuit current (I_{sc}) of 3.6 A.

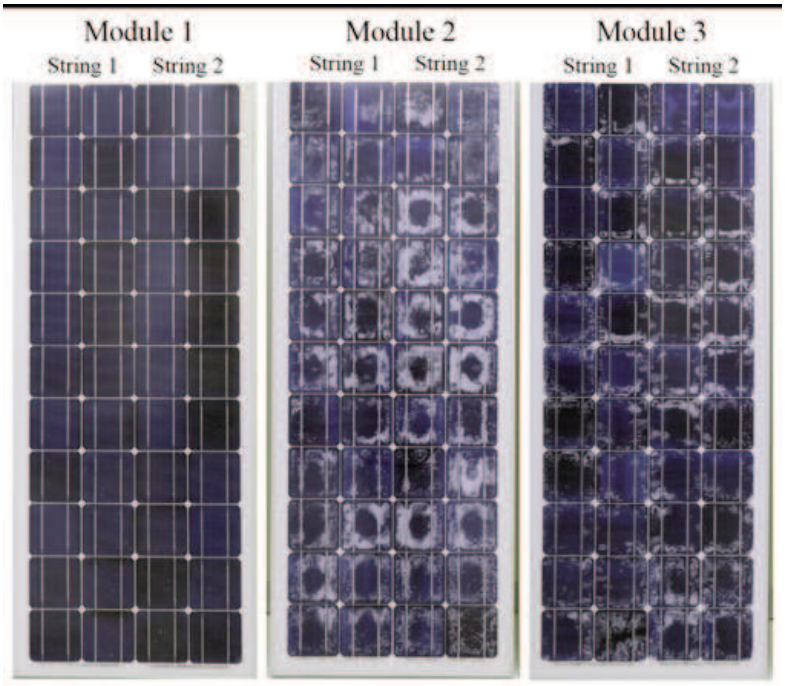

Figure 4: Photographs of Module 1 (reference), Module 2 and Module 3

3. Results

3.1. Outdoor I-V curves

The performance parameters of the three modules and the manufacturer's specifications are given in Table 1. The reference module 1 has the best power and current output as expected, with a measured P_{max} of 64.6 W. The variation from the specified 65 W is most likely due to the small micro-cracks that were only visible in the EL image.

Table 1: The performance parameters of the three modules with the manufacturer's specifications

	V_{oc} [V]	I_{sc} [A]	P_{max} [W]
Module 1	25.4	3.6	64.6
Module 2	25.8	3.4	55.1
Module 3	25.7	3.4	54.1
Manufacturer's specifications	25.0	3.6	65.0

The I-V curves of the three modules, with bypass diodes connected, and those of the individual strings without bypass diodes are shown in Figure 5. Module 1 has no visible damage or degradation as seen in the photograph of the module, Figure 4. The I-V curves of module 1 with bypass diodes and its individual strings are shown in Figure 5. The cells in each string of module 1 are evenly matched and produce the same current and thus the I-V curves of each string are identical. When the strings are current matched the same current is generated, so the bypass diodes that are parallel connected across the cell strings are not activated. The voltages of the two strings add at equal currents, resulting in the I-V curve of the whole module. The module is, therefore, used as a reference module for comparison of the performance and cell mismatch of the other modules.

The I-V curves of module 2 and its cell strings are shown in Figure 6. String 1 has a lower current and power output than string 2, resulting in current mismatch between the two strings. String 1 is reverse biased by a voltage greater than the bypass diode's turn-on voltage, which activates the bypass diode across string 1. The step in the module I-V curve, at about 7 V, is due to the activation of the bypass diode and the bypassing of string 1 and thus the Isc of the module is determined by the Isc of string 2. If bypass diodes are not used the module's Isc will be limited by string 1's Isc and thus by the

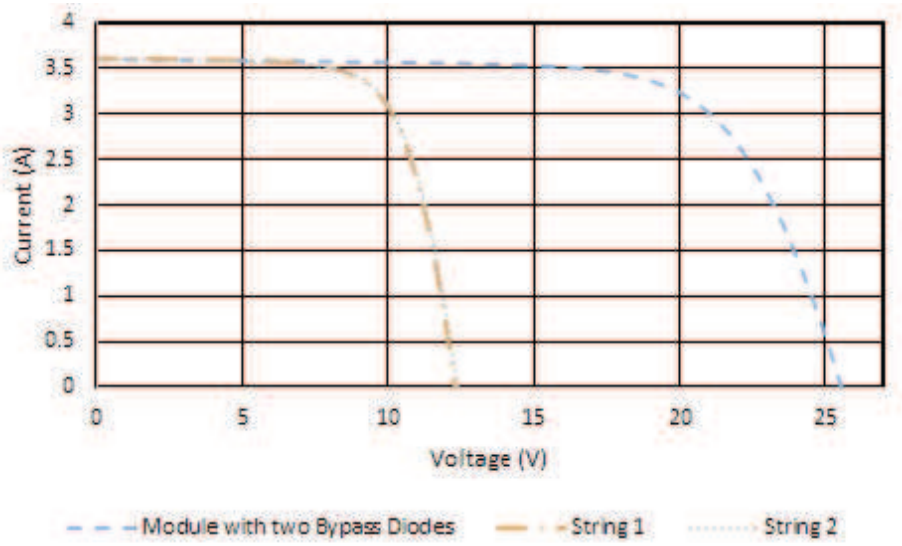

Figure 5: The I-V curves of module 1 and its individual strings

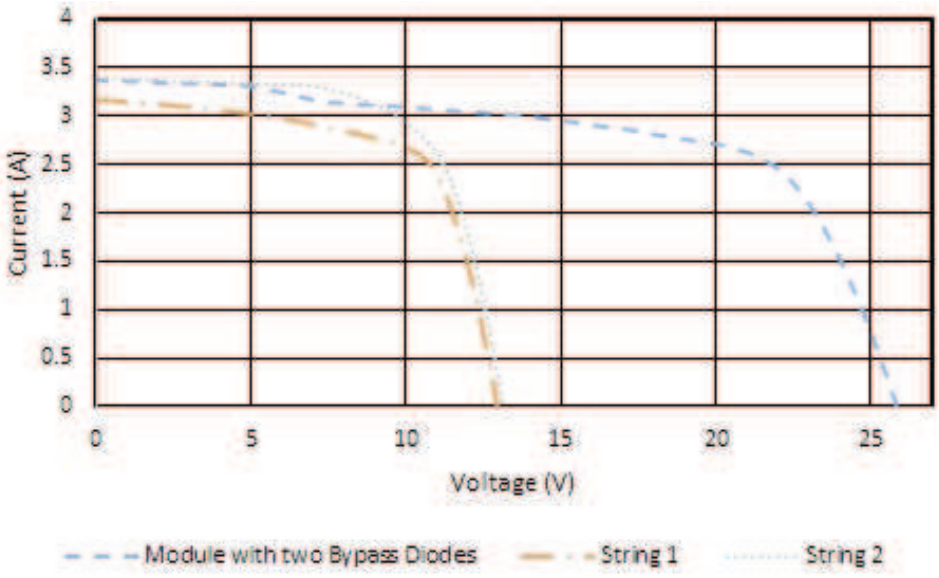

Figure 6: The I-V curves of module 2 and its individual strings

weakest cell in the string.

The I-V curves of module 3 and the individual strings are shown in Figure 7. The current of the two strings is matched at Isc and thus neither of the bypass diodes are activated. However, in the region before the "knee", between 2 and 11 V, the current of string 1 is lower than string 2. This could be due to a combination of cell mismatch effects and shunt resistance as this region of the I-V curve is influenced by shunt resistance in the cell and module. In an ideal solar cell, the resistance due to shunting across the p-n junction should be infinite but due to manufacturing defects shunting can occur. Low shunt resistance results in an alternative current path for light generated current thus reducing the current of the cell. At low voltage levels the impact of parallel shunt resistance is significant.

3.2. EL images

The EL images of all the modules in the study are shown in Figure 8. Figure 8(a), the EL image of module 1, corroborates the results of the I-V curve as there are no large severely damaged areas visible and the two cell strings are evenly matched. Common cell defects, such as finger defects and micro-cracks that affect small areas can be detected. Finger defects occur due to a break across the contact fingers across the cell resulting in the area between the fingers of the cell having decreased electrical contact and appearing darker in the EL image. Finger defects occur in the majority of the cells in this module, possibly due to problems in the manufacturing process. Micro-cracks are visible in highlighted cells C8 and C9 in module 1. The micro-cracks indicated in C9 are visible in the EL

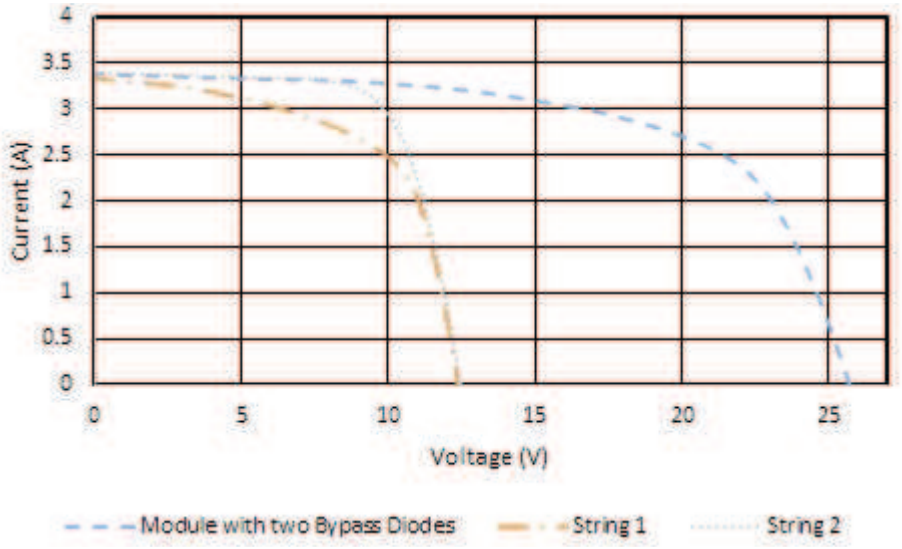

Figure 7: The I-V curves of module 3 and its individual strings

but do not cause inactive areas in the cells (Köntges *et al.*, 2011). This type of crack most likely occurred during the manufacturing process and would not be detected in the I-V module testing process as they do not result in a significant drop in cell performance. With time and thermal cycling these cracks have the potential to spread and result in performance degradation. The micro-cracks in the corner of the cell C8 completely removes an area of the cell from electrical contact resulting in a completely dark area in the EL image. This inactive area indicates that this area of the cell has poor photo-response lowering the performance of the cell. This decrease, however, does not significantly affect the performance of the module because of the small area affected and is therefore not observed in the I-V curve.

The EL image of module 2 is shown in Figure 8(b) and reveals several defects and large inactive areas due to broken cells. The effect of the degradation in the anti-reflective coating is visible in the EL image as areas that have been discoloured correspond with areas of lower EL signal intensity. This could be due to the discolouration of the anti-reflective coating that blocks the EL signal from being detected. Either way, this degradation results in poor photo-response and, ultimately, performance degradation in the affected areas. In cell B4 a micro-crack has prevented electrical contact between the one side of the cell and the other. The high current density in the one third of the cell results in a higher intensity EL signal. Cells A7, B7, B8, C8 are severely cracked. These cracks cause large inactive areas which result in lower performance of these cells. The cause of this damage is most likely due to mechanical damage as the cracks line up with scratches that have been observed

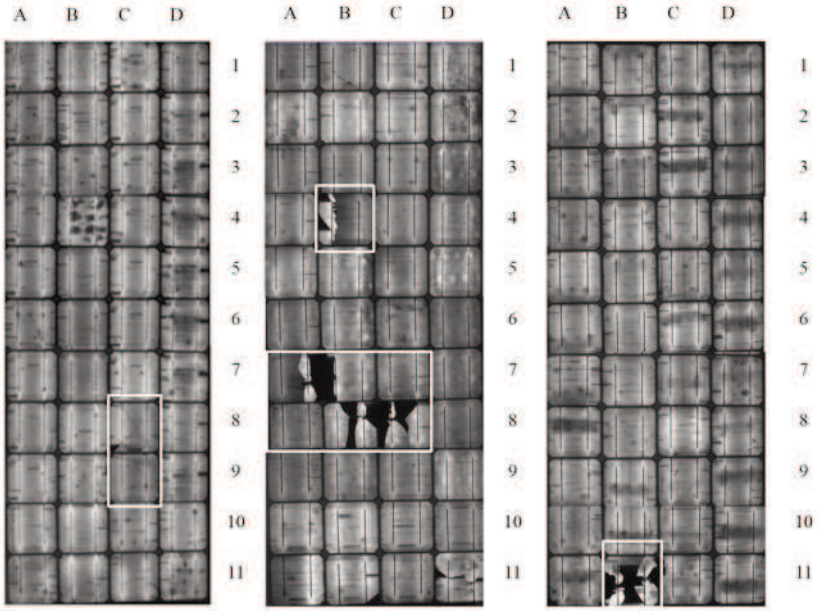

Figure 8: The EL images of a) module 1, b) module 2 and c) module 3

along the back surface of the module. The EL images explain the mismatch seen in the I-V curves of the two strings as string 1 has more inactive cell area than string 2 and thus lower current output.

The EL image of module 3 is shown in Figure 8(c). Cell B11 is the severely damaged with cracks resulting in large inactive areas which lower the performance of the module. This damaged cell is responsible for the lower performance of string 1 compared with string 2 obseved in the I-V curves. While this damaged cell doesn't lower the Isc of string 1, it does contribute to the cell mismatch and shunting observed in the I-V curve.

4. Summary and conclusion

Electroluminescence is used as a fast and effective technique in identifying defects and degradation in these three PV modules. It is able to quickly detect cell defects that would not be detected in visual module inspection or I-V curve measurement. These defects can explain why some modules, such as module 1, appear undamaged but have lower power output than expected. Defects in a module can be detected at the manufacturing stage enabling manufacturers to increase the reliability of PV modules. Cell mismatch can be observed in the I-V curves of a module but the EL image of the module allows the identification of cell defects and the exact nature and position of the defects may also be determined.

Despite the EL of module 2 indicating that it has several severely cracked cells, the performance parameters of modules 2 and 3 are very similar. The bypass diodes in module 2 increases the Isc of module 2, and thus the power outputs of module 2 and 3 are very similar despite module 2 having more damaged cells. The EL images of module 2 clearly indicate that the cell mismatch which is seen in the I-V curve of the module is due to cracked cells and inactive areas. These defects result in a lower current output in one string which is visible in the I-V curve. Similarly, a damaged cell only visible in the EL image of module 3 could be responsible for the lower performance and shunting visible in the I-V curve of the module.

References

Alonso-García M.C. and Ruíz J.M. (2006). Analysis and modelling the reverse characteristic of photovoltaic cells. *Solar Energy Materials and Solar Cells* 90: 1105-1120.

Camino-Villacorta M., Coello J, Pérez L., *et al*. (2012). Comparative Analysis of Electroluminescence, IR Thermography and Visual Inspection on c-Si Modules. *27th European Photovoltaic Solar Energy Conference and Exhibition.* Frankfurt, Germany.

Chaturvedi P., Hoex B. and Walsh T.M. (2013). Broken metal fingers in silicon wafer solar cells and PV modules. *Solar Energy Materials and Solar Cells* 108: 78-81.

Fuyuki T. and Kitiyanan A. (2008). Photographic diagnosis of crystalline silicon solar cells utilizing electroluminescence. *Applied Physics A* 96: 189-196.

Fuyuki T, Kondo H., Kaji Y., *et al.* (2007). Analytic findings in the electroluminescence characterization of crystalline silicon solar cells. *Journal of Applied Physics* 101: 023711.

Fuyuki T., Kondo H., Yamazaki T., *et al.* (2005). Photographic surveying of minority carrier diffusion length in polycrystalline silicon solar cells by electroluminescence. *Applied Physics Letters* 86: 262108.

Gabor A.M., Ralli M., Montminy S., *et al.* (2006). Soldering Induced Damage to Thin Si Solar Cells and Detection of Cracked Cells in Modules. *21st European Photovoltaic Solar Energy Conference.* Dresden, Germany.

IEAPVPS (2014). Performance and Reliability of Photovoltaic Systems Subtask 3.2:Review of Failures of Photovoltaic Modules. IEA International Energy Agency.

Kajari-Schröder S., Kunze I, Eitner U., *et al.* (2011). Spatial and orientational distribution of cracks in crystalline photovoltaic modules generated by mechanical load tests. *Solar Energy Materials and Solar Cells* 95: 3054-3059.

King D.L., Dudley J.K. and Boyson WE. (1996). PVSIM© : A Simulation Program for Photovoltaic Cells, Modules, and Arrays. *25th IEEE PVSC.* Washington, DC.

Kirchartz T., Helbig A., Reetz W., *et al.* (2009). Reciprocity between electroluminescence and quantum efficiency used for the characterization of silicon solar cells. *Progress in Photovoltaics: Research and Applications* 17: 394-402.

Köntges M., Kunze I., Kajari-Schröder S., *et al*. (2011). The risk of power loss in crystalline silicon based photovoltaic modules due to micro-cracks. *Solar Energy Materials and Solar Cells* 95: 1131-1137.

Köntges M, Siebert M, Illing R, *et al.* (2014). Influence of Photovoltaic-module Handling on Solar Cell Cracking. *29th European Photovoltaic Solar Energy Conference and Exhibition.* Amsterdam, the Netherlands, 2276-2282.

Mansouri A., Zettl M., Mayer O., *et al*. (2012). Defect detection in photovoltaic modules using electroluminescence imaging. *27th European Photovoltaic Solar Energy Conference and Exhibition.* Frankfurt, Germany.

Meyer E.L. and van Dyk E.E. (2004). Assessing the Reliability and Degradation of Photovoltaic Module Performance Parameters. *IEEE Transaction on Reliability* 53: 83-92.

NIH. (2004). *ImageJ*. Available at: http://rsbweb.nih.gov/ij/.

Paggi M. and Sapora A. (2013). Numerical Modelling of Microcracking in PV Modules Induced by Thermo-mechanical Loads. *Energy Procedia* 38: 506-515.

Sander M., Dietrich S., Pander M., *et al.* (2013). Systematic investigation of cracks in encapsulated solar cells after mechanical loading. *Solar Energy Materials and Solar Cells* 111: 82-89.

Vorster F.J. and van Dyk E.E. (2005). Current-voltage characteristics of high-concentration, photovoltaic arrays. *Progress in Photovoltaics: Research and Applications* 13: 55-66.
Würfel P., Trupke T., Puzzer T., *et al.* (2007). Diffusion lengths of silicon solar cells from luminescence images. *Journal of Applied Physics* 101: 123110.

Received 9 January 2014; revised 14 August 2015